Tensile drawing of poly(aryl ether ether ketone): 1. Birefringence, infra-red dichroism and shrinkage-stress measurements

Véronique Bassigny and Roland Séguéla*
Laboratoire de Structure et Propriétés de l'Etat Solide, URA CNRS 234, Université de Lille I, 59655 Villeneuve d'Ascq Cedex, France

and François Rietsch
Laboratoire de Caractérisation des Matériaux Polymères et Composites, Ecole Universitaire d'Ingénieurs de Lille, Université de Lille I, 59655 Villeneuve d'Ascq Cedex, France

and Bruno Jasse
Laboratoire de Physicochimie Structurale et Macromoléculaire, URA CNRS 278, ESPCI, 10 rue Vauquelin, 75231 Paris Cedex 05, France
(Received 29 September 1992; revised 15 January 1993)

Birefringence, infra-red dichroism and shrinkage-stress data of poly(aryl ether ether ketone) (PEEK) uniaxially drawn above the glass transition have been analysed in the framework of the theory of rubber elasticity. It is shown that PEEK chains having a molecular weight $M_n \approx 13000$ only contain three entanglements per chain on average. The very low level of shrinkage stress of the samples having a draw ratio below the threshold of strain-induced crystallization is perfectly consistent with a weakly entangled network. The birefringence *versus* stress curve discloses an orientation-dominated regime at low strains and a deformation-dominated regime starting from the onset of the strain-induced crystallization. The length of the random link, $L = 1.8$ nm, is in very good agreement with the one that can be theoretically predicted for the stiff-chain polymer relatives, poly(ethylene terephthalate), polycarbonate and poly(phenylene oxide). A value for the intrinsic birefringence of the amorphous phase, $\Delta n_a^\circ = 0.38 \pm 0.04$, is also reported.

(Keywords: poly(aryl ether ether ketone); birefringence; infra-red dichroism; thermal shrinkage; entanglements; random link)

INTRODUCTION

Poly(aryl ether ether ketone), commonly PEEK, is a high-performance semicrystalline thermoplastic polymer[1]. Its very high thermal stability and strong resistance to solvents make it a good candidate as the matrix for fibre-reinforced composites. The large number of unsubstituted phenyl groups in the monomer formula (-ϕ-O-ϕ-O-ϕ-CO-) results in both high chain stiffness and strong interactions between neighbouring chains, which are responsible for the main physical properties of the polymer, namely high glass transition temperature ($T_g \approx 150$°C), high melting point ($T_f \approx 350$°C) and good crystallization capability. Concerning the crystallization behaviour, PEEK departs strongly from its structural relatives bisphenol A polycarbonate and poly(2,6-dimethyl-1,4-phenylene oxide), which have very little propensity to form crystalline structures[2]. It is, however, much more similar to poly(ethylene terephthalate), which has significantly lower thermal properties.

Investigation of the strain-orientational behaviour at temperatures above the glass transition is an important step in the general understanding of the mechanical properties of stiff-chain polymers, notably as concerns the set-up of the processing conditions and the characterization of use properties.

EXPERIMENTAL

The Stabar K200 polymer under investigation was an amorphous cast film from ICI with thickness of about 50 μm. It was perfectly isotropic and exhibited no measurable shrinkage upon heating above the glass transition temperature. A semicrystalline material having a nominal crystallinity of 29% was also prepared by isothermal treatment of amorphous sheets for 1 h at 170°C.

The drawing experiments have been carried out with dumbbell-shaped samples (having 25 mm gauge length and 5 mm width, respectively) that were cut out from the sheets with a cutting punch. The samples were thermally

* To whom correspondence should be addressed

0032-3861/93/194052-08

homogenized in the oven of an Instron tensile testing machine at the temperature of the drawing experiment for a period of 10 min before drawing. The cross-head speed was 50 mm min^{-1}. At the end of the drawing, the samples were rapidly cooled down below the glass transition temperature in air within about 1 min, at constant length, prior to unloading. The amorphous samples were deformed at 160°C, which is in the mid-range between the peak temperature of the cold-crystallization exotherm, $T_c \approx 175$°C, and the temperature of the glass transition heat capacity jump, $T_g \approx 145$°C. It is worth noticing that no thermal crystallization occurs in the amorphous samples during the pre-drawing treatment as judged from crystallinity measurements on samples treated at the same temperature for periods up to 1 h. The crystalline samples were drawn at 185°C.

Birefringence measurements have been carried out on a Wild–Leitz polarizing microscope equipped with an Ehringhaus compensator. For the partially crystallized samples, the overall birefringence is assumed to obey Stein's additivity law[3,4]:

$$\Delta n = \Delta n_a + \Delta n_c = \Delta n_a^\circ f_a (1 - X_c) + \Delta n_c^\circ f_c X_c \qquad (1)$$

where Δn_a° and Δn_c° are the intrinsic birefringences of the perfectly oriented amorphous and crystalline phases, respectively, f_a and f_c are the amorphous and crystalline orientation functions, respectively, and X_c is the degree of crystallinity.

Densities have been determined by the flotation technique in a gradient column of sodium nitrate solution made according to the standard ASTM method D1505-68 at 23°C[5]. The weight fraction crystallinity was assessed from the relation:

$$X_c = \frac{\rho_c}{\rho}\left(\frac{\rho - \rho_a}{\rho_c - \rho_a}\right) \qquad (2)$$

The value generally admitted for the amorphous phase density is $\rho_a = 1.264$ g cm^{-3} (refs. 6–8). On the other hand, the density of the crystalline phase seems to depend on the crystallization temperature[9,10], and the value for a very low crystallization temperature, such as the drawing temperature of the experiments reported presently ($T_d = 160$°C), is $\rho_c = 1.367$ g cm^{-3}.

Thermal behaviour has been investigated by means of differential scanning calorimetry (d.s.c.), using a Perkin–Elmer DCS-7-Delta apparatus. The heating rate was 10 K min^{-1} and the sample weight was in the range 5–10 mg. The melting of indium and zinc samples was used to calibrate the temperature and the heat flow scales at the same heating rate. The weight fraction crystallinity of the PEEK samples prior to the d.s.c. scan was calculated from the equation:

$$X_c = \frac{\Delta H_f}{\Delta H_f^\circ} - \frac{\Delta H_c}{\Delta H_c^\circ} \qquad (3)$$

where the first term stands for the whole weight fraction of crystals that melt in the d.s.c. endotherm and the second term stands for the weight fraction of the material that recrystallizes during the d.s.c. scan. ΔH_f and ΔH_c are the actual enthalpies of fusion and crystallization of the materials under investigation. ΔH_f° and ΔH_c° are the enthalpies of fusion and crystallization of an infinite and perfect crystal at the temperatures of the melting endotherm and the cold-crystallization exotherm, respectively. Despite the previously established temperature dependence of the enthalpy of fusion of PEEK[11], it has been assumed that $\Delta H_f^\circ = \Delta H_c^\circ = 130$ J g^{-1} (ref. 6), as is commonly done, in order to allow comparison with literature data.

Infra-red (i.r.) dichroism measurements have been carried out on a Nicolet 205 Fourier-transform infra-red spectrometer provided with a Specac gold-wire grid polarizer. The infra-red spectra were recorded at 2 cm^{-1} resolution from 32 scans. The second-order moment of the orientation distribution function, $\langle P_2(\cos\theta)\rangle$, otherwise Hermann's orientation function:

$$f(\cos\theta) = \tfrac{3}{2}\langle\cos^2\theta\rangle - \tfrac{1}{2} \qquad (4)$$

where θ is the angle between the local chain axis and the draw direction, has been determined for the crystalline phase and the overall material from the dichroic ratio of the appropriate i.r. bands from the relation:

$$f = \frac{(D-1)(D_0+2)}{(D+2)(D_0-1)} \qquad (5)$$

The dichroic ratio D of a given infra-red band is the ratio of the absorbances measured parallel and perpendicular to the draw direction, $D_0 = 2\cot^2\alpha$ being the dichroic ratio for the perfect alignment of the chains parallel to the fibre axis and α being the angle between the transition moment vector and the local chain axis[12–14].

Considering the molecular mobility induced by the ether and ketone linkages, which affords different conformational structures, the longest chain axis that can be defined is the axis joining the centres of two adjacent aromatic rings. This is perfectly supported by the extended structure of the PEEK chain in the most stable conformation of the crystalline state[6–10].

Different absorption bands of PEEK can be used in order to assess chain orientation. In the present case, many bands are too strong to be used on account of the thickness of the samples. Two absorption bands, at 1012 and 952 cm^{-1} are characteristic of the overall chain orientation[15–17]. The 1012 cm^{-1} band is assigned to the ν_{18a} symmetric mode of the phenyl ring, the dipole moment vector of which lies on the C1–C4 axis and makes an angle $\alpha = 30°$ with respect to the chain axis[17,18]. On the other hand, the 952 cm^{-1} absorption band remains unassigned. However, the values of the dichroic ratio are very close to those of the 1012 cm^{-1} absorption band, indicating that the 952 cm^{-1} absorption band more likely originates from an in-plane vibration mode of the benzene rings rather than an out-of-plane vibration mode as suggested by Jonas *et al.*[17]. From the values of the orientation functions deduced from the 1012 cm^{-1} band, we obtain an angle $\alpha \approx 28°$ for the 952 cm^{-1} band, using the relation:

$$\langle P_2(\cos\theta)\rangle_{1012} = \left(\frac{(D-1)(D_0+2)}{(D+2)(D_0-1)}\right)_{952} \qquad (6)$$

which assumes the same orientation function for the two bands.

The crystalline orientation function can be deduced from the absorption band that appears at 965 cm^{-1}. It is to be mentioned that the assignment of this absorption band is controversial. Nguyen and Ishida[15,16] together with Chalmers *et al.*[19] have shown a clear correlation between the crystalline phase and this vibrational mode. On the other hand, Jonas *et al.*[17] suggested that the 965 cm^{-1} band could originate from a normal vibration

mode of short segmental conformations, which are favoured in the crystalline phase but can also be present in strained chains of the amorphous regions. We nevertheless used this absorption band to determine the crystalline orientation, taking the angle $\alpha = 30°$ because of its very similar dichroic behaviour to that of the 1012 and 952 cm^{-1} bands. It will be shown in the next section that this choice is advocated by X-ray data from other authors.

Shrinkage-stress experiments have been performed on a previously described apparatus made in the laboratory[20]. The 50 N Instron cell was accurately calibrated over the range of the force measurements, i.e. from -1 to 5 N. The slight compressive force recorded for the samples having low draw ratios is due to the thermal expansion consecutive to the heating from room temperature to the shrinkage temperature $T_s = 160°C$. The temperature measured with a thermocouple in contact with the sample surface was regulated at the desired value within less than 20 s owing to a temperature-controlled air flow delivered by a heating gun. The determination of the shrinkage force was made from the difference between the maximum signal due to the maximum entropic response before slippage of the chains and the minimum signal due to thermal expansion of the samples.

Small-angle X-ray scattering measurements have been performed photographically on a Luzzati–Baro goniometer following a previously described procedure[21].

RESULTS AND DISCUSSION

Strain-induced crystallization

Figure 1 shows typical d.s.c. heating curves for samples drawn from the amorphous state, for various values of the draw ratio, λ. Crystallization under strain is only partial and most of the samples exhibit a more or less pronounced cold-crystallization phenomenon during the d.s.c. scan. The locations of the crystallization peak at $T_c^{max} \approx 175°C$ and the glass transition heat capacity jump at $T_g \approx 145°C$ for the isotropic sample can be used to estimate the molecular weight, $M_n \approx 13\,000$, according to the correlation reported by Day *et al.*[22]. The crystal weight fractions computed for the samples prior to the d.s.c. scan according to the method proposed in the experimental part are collected in *Figure 2* together with the values assessed from the density data at 23°C. Both methods show that the onset of the strain-induced crystallization for the amorphous samples occurs at about $\lambda = 1.6$ when the chains have undergone a sufficient orientation. In the case of the crystallized samples, the crystallinity increases only slightly with the draw ratio. It has been pointed out that strain-induced crystallization under conditions for which no crystallization occurs in the quiescent melt results from a significant lowering of the activation energy due to the chain orientation, which improves the rate of formation of primary nuclei[23,24]. The strong influence of the flow rate on the kinetics without development of macroscopically oriented structures[24] is an indication that local orientation of segments due to chain stiffness takes place instead of network extension.

Birefringence and infra-red dichroism

The strain-induced birefringence reported in *Figure 3* as a function of the draw ratio seems to level off for

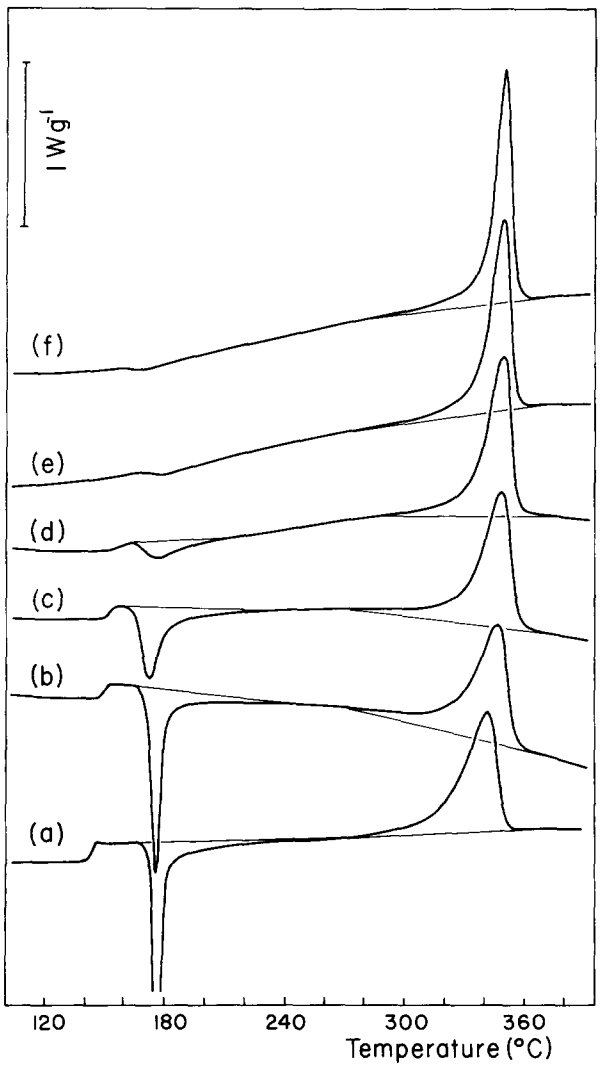

Figure 1 D.s.c. heating curves of samples drawn from the amorphous state for various values of the draw ratio, λ: (a) $\lambda = 1.00$; (b) $\lambda = 1.32$; (c) $\lambda = 1.84$; (d) $\lambda = 2.27$; (e) $\lambda = 2.80$; (f) $\lambda = 3.40$

$1.3 < \lambda < 1.8$ after a sudden increase at very low strains. This is relevant to a creep effect due to the unravelling of the weakly entangled chains in the first stage of the straining of the chain network. This is due to the lack of physical crosslinking of the low-molecular-weight chains prior to the strain-induced crystallization effect. This is supported by the comparison with the strain-induced birefringence of crystallized PEEK, which does not show the levelling-off effect in the intermediate strain range owing to the presence of crystals before deformation. The chain unravelling phenomenom will be further discussed below and also in the accompanying paper concerned with the modelling of the orientational behaviour. At the onset of the strain-induced crystallization, for $\lambda \approx 1.8$, a strong increase of the birefringence occurs, indicating that the chains are efficiently extended as soon as enough crystals are formed to prevent chain slippage.

The infra-red dichroism data have been reported in *Table 1*, which shows the crystalline and overall average orientation functions, f_c and f_{av}. In order to modulate the errors on the determination of f_{av}, both the 1012 and the 952 cm^{-1} bands have been used despite the fact that the angle $\alpha = 28°$ of the second band has been estimated from the orientation function of the former band. The amorphous orientation function f_a was computed from

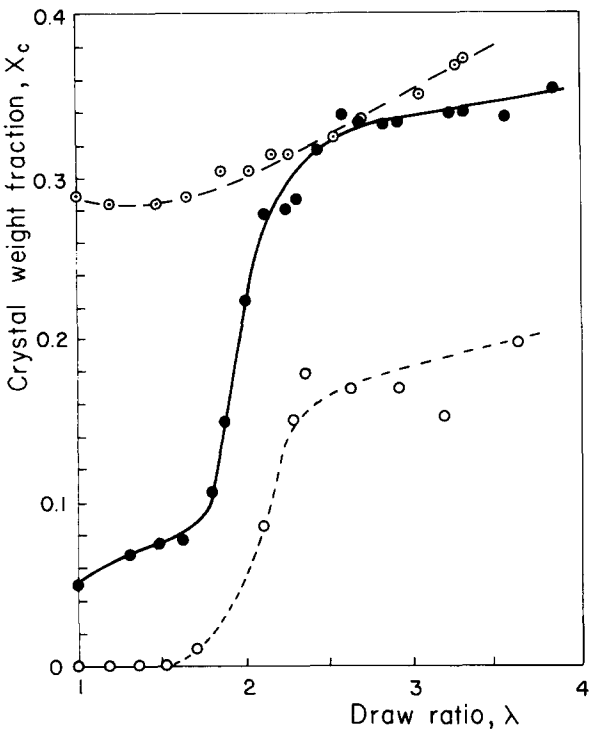

Figure 2 Crystal weight fraction as a function of the draw ratio, λ: (●) data from d.s.c. and (○) data from the densities for samples drawn from the amorphous state; (⊙) data from d.s.c. for isothermally crystallized samples

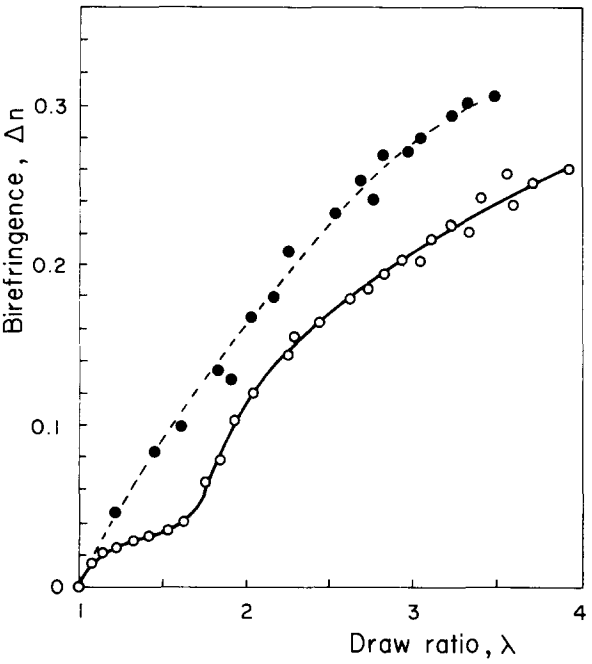

Figure 3 Strain-induced birefringence, Δn, as a function of draw ratio, λ: (○) samples drawn from the amorphous state; (●) isothermally crystallized samples

the relation:

$$f_{av} = X_c f_c + (1 - X_c) f_a \quad (7)$$

using an average value of f_{av} at every draw ratio λ (see *Table 1*).

The crystalline orientation function levelling-off at the rather moderate value $f_c = 0.67 \pm 0.02$ for $2.2 < \lambda < 3.43$ is a quite surprising result in comparison with what is usually observed with flexible-chain polymers. However, this is perfectly consistent with previous X-ray diffraction measurements of Lee *et al.*[25] on PEEK rods extruded at 310°C, which showed that $f_c \approx 0.65$ at $4 < \lambda < 5$. *Figure 4* shows the wide-angle X-ray diffraction patterns of samples of draw ratios $\lambda = 2.0$ and $\lambda = 3.7$ showing significant azimuthal scattering of the strong (1 1 0) and (2 0 0) reflections indicative of a not-perfect *c*-axis orientation parallel to the draw direction. The qualitative similarity of the two patterns is consistent with the very small change of the f_c values from infra-red dichroism measurements in the range of the draw ratios of the X-ray patterns (see *Table 1*). Besides, the fact that the pattern

Table 1 Crystalline, amorphous and average orientation functions, f_c, f_a and f_{av}, from infra-red dichroism measurements

Draw ratio λ	f_{av} (952 cm^{-1})	f_{av} (1012 cm^{-1})	f_c (965 cm^{-1})	f_a
1.21	0.06	0.06	0.16	0.05
1.37	0.09	0.05	0.19	0.06
1.63	0.15	0.17	0.25	0.15
1.85	0.20	0.19	0.44	0.17
2.07	0.43	0.43	0.65	0.35
2.27	0.45	0.42	0.66	0.34
2.81	0.55	0.57	0.66	0.52
3.43	0.63	0.63	0.69	0.60

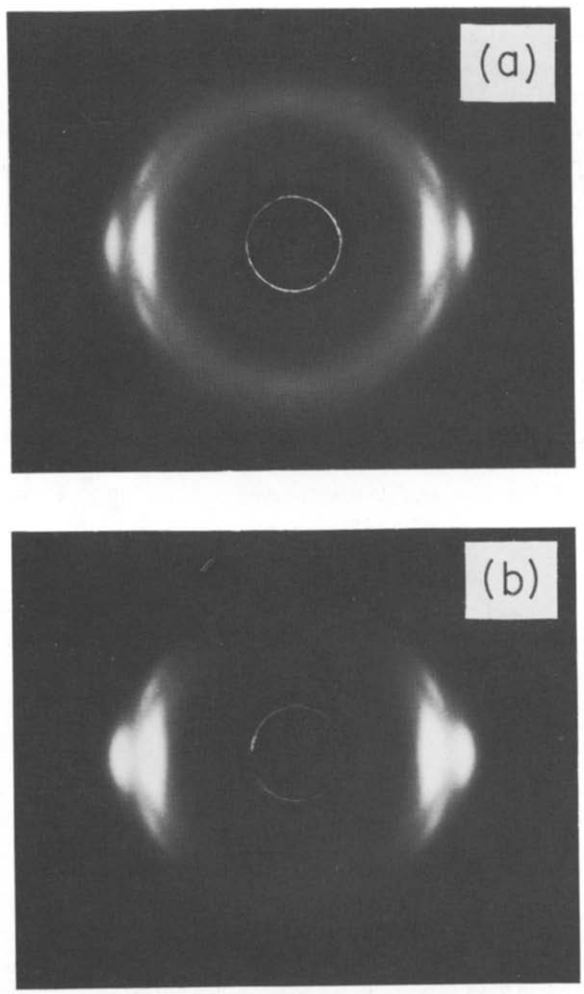

Figure 4 Wide-angle X-ray diffraction patterns of samples of draw ratios (a) $\lambda = 2.0$ and (b) $\lambda = 3.7$ (the draw axis is vertical)

of *Figure 4* at $\lambda = 3.7$ is very similar to the pattern reported by Lee *et al.* for an extruded rod of draw ratio $\lambda = 3.8$ indicates that the samples investigated in the two studies follow the same orientational behaviour, and this provides better support to the comparison made previously between f_c values from X-ray diffraction data reported by the above authors and our own data from infra-red dichroism.

The unusually large f_a values of *Table 1* are, on the other hand, perfectly consistent with the negative thermal expansivity coefficient reported for PEEK samples drawn to the ultimate draw ratio[25,26], which is relevant to a high molecular orientation in the amorphous phase.

The amorphous contribution to the birefringence, $\Delta n_a/(1-X_c)$, for samples drawn from the amorphous state is plotted in *Figure 5* as a function of the draw ratio. The values of Δn_a are computed from equation (1), using the overall birefringence values (*Figure 3*) and an average value of the crystalline orientation functions obtained from the two infra-red bands (*Table 1*). The two curves of *Figure 5* are very close, indicating that the choice of the crystallinity values from d.s.c. or density measurements is of little importance. From the data of *Figure 5* together with the amorphous orientation functions of *Table 1*, one can assess a value for the amorphous intrinsic birefringence, $\Delta n_a^\circ = 0.38 \pm 0.04$. This value is significantly higher than the value estimated by Cakmak[27], $\Delta n_a^\circ = 0.281$, which was determined from the crystalline intrinsic birefringence, $\Delta n_c^\circ = 0.310$, with the assumption of a simple density dependence. In support of the presently determined value of Δn_a° it is worth recalling the well known internal field effect of the crystal, which reduces the optical anisotropy of the chemical bonds in the crystalline state compared with the amorphous state for various semicrystalline polymers such as poly(ethylene terephthalate)[12], polypropylene[12] and polyethylene[28]. Besides, using the Δn_a° value of Cakmak for determining the amorphous orientation function from the amorphous birefringences of *Figure 5* would give a value $f_a \approx 0.92$ for the higher draw ratio

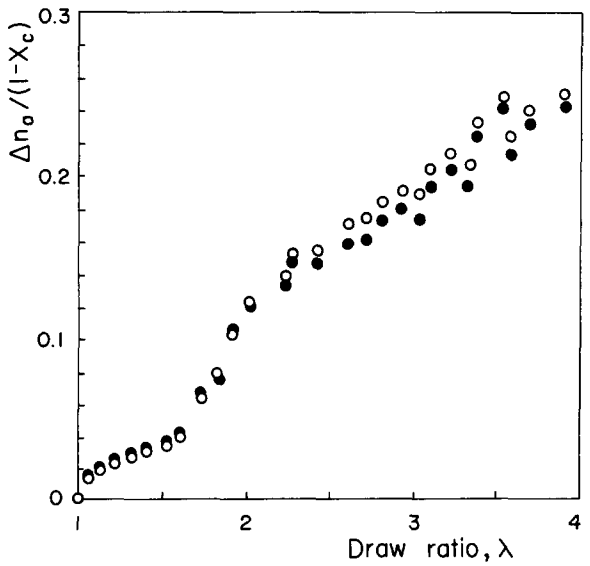

Figure 5 Amorphous birefringence contribution, $\Delta n_a/(1-X_c)$, as a function of draw ratio, λ, for the samples drawn from the amorphous state. The data are computed with crystallinity value assessed from d.s.c. (●) and from densities (○)

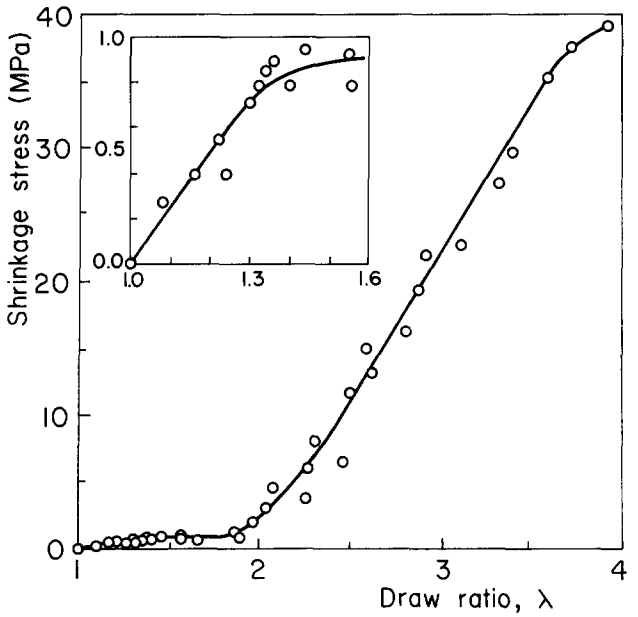

Figure 6 Shrinkage stress, σ, as a function of draw ratio, λ, for samples drawn from the amorphous state. The insert shows an enlarged view of the low-strain region

$\lambda = 3.43$, which seems very unlikely with regard to the crystalline orientation function $f_c \approx 0.69$ (*Table 1*). In this connection, it is also worth noticing that Choy *et al.*[26] have previously stressed that Cakmak's Δn_a° value was too low to account properly for the orientation behaviour of PEEK.

Thermal shrinkage

Figure 6 shows the shrinkage stress at 160°C as a function of the draw ratio. The stress plateau in the range $1.3 < \lambda < 2.0$ is a conspicuous effect of the unravelling of the weakly entangled chains before the onset of the strain-induced crystallization, which requires a sufficient segment orientation to start as previously suspected from the birefringence behaviour. The strain hardening that appears in *Figure 6* for $\lambda > 2.0$ is evidence of the efficiency of strain-induced crystallization as a physical crosslinking agent.

According to the statistical chain theory of rubber elasticity, the stress–strain behaviour of a polymer above the glass transition temperature is given by the well known relation, which accounts for the effect of dangling chain ends[29]:

$$\sigma = \frac{\rho RT}{M_e}(\lambda^2 - \lambda^{-1})\left(1 - \frac{2M_e}{M_n}\right) \tag{8}$$

where σ is the true stress, ρ is the density of the polymer at the temperature T of the experiment and M_e is the average molecular weight between entanglements. The Young's modulus:

$$E = \lim_{\lambda \to 1} \frac{\partial \sigma}{\partial \lambda} = 3\frac{\rho RT}{M_e}\left(1 - \frac{2M_e}{M_n}\right) \tag{9}$$

was determined from the slope at the origin of the best-fitting linear relationship in the strain range $1.0 < \lambda < 1.3$ of the shrinkage stress *versus* draw ratio plot of *Figure 6*. From the modulus value $E = 2.5 \pm 0.3$ MPa

that was thus deduced for rubbery PEEK at $T=160°C$, the value $M_e \approx 2000$ has been determined by taking the density at room temperature, and considering the fact that thermal expansion between room temperature and the shrinkage experiment temperature has a very low effect compared with the accuracy of the mechanical data[26]. Taking into account the number-average molecular weight $M_n \approx 13\,000$ of the polymer, it can be concluded that there are only three entanglements per chain on average. Another interesting remark is that the contour length of the chain between entanglements, $l_e = 15.6$ nm, is very close to the one reported[30,31] for the PEEK structural analogue poly(2,6-dimethyl-1,4-phenylene oxide) (PPO), $l_e = 16.5$ nm. It is worth mentioning that substantially greater values of the PPO chain length between entanglements have also been reported[31,32], but no explanation has been provided for this discrepancy.

Combination of birefringence and shrinkage-stress measurements affords determination of the stress-optical coefficient of the amorphous phase. The amorphous contribution to the birefringence, $\Delta n_a/(1-X_c)$, for samples drawn from the amorphous state is plotted in *Figure 7* as a function of the shrinkage stress, σ. The relevance of the plot of *Figure 7* relies on the assumption of a uniform stress distribution over the crystalline and amorphous phases, i.e. a Reuss average or series association model[12,33–35]. It is worth mentioning that in the case of semicrystalline polyethylene this model has proved to be more satisfactory than the parallel association model for fitting elastic modulus data, for isotropic as well as for oriented samples. The curve of *Figure 7* is composed of two roughly linear domains, the slope in the low-stress region of the curve being twice as large as that in the high-stress range. This behaviour is far different from that reported for poly(ethylene terephthalate) (PET)[36], which displays a linear variation of birefringence at low stress and a subsequent sigmoidal increase with increasing stress. In the case of PET[36], as well as for poly(methyl methacrylate) (PMMA)[37], the strain-independent stress-optical coefficient in the initial part of the Δn *versus* σ curve has been treated in the framework of the polymer network deformation model of Kuhn and Grün[38] for flexible chains. For a uniaxial extension, the following relation holds for amorphous polymers at temperatures around the glass transition:

$$\frac{\Delta n}{\sigma} = \frac{2\pi}{45kT}\frac{(n^2+2)^2}{n}N(a_1-a_2) \qquad (10)$$

where k is the Boltzmann constant, n is the mean refractive index of the polymer, N is the number of elastically active chains per unit volume, and a_1 and a_2 are the polarizabilities of the random link parallel and perpendicular to its backbone axis, respectively.

In the case of PEEK, the change in slope of *Figure 7* is strikingly similar to the flow birefringence behaviour of polymer solutions as a function of increasing viscosity or shear stress[39,40]. Generally, an orientational birefringence regime first occurs followed by a deformational birefringence regime having a lower variation slope. The higher the rigidity of the chain, the larger is the extent of the orientational birefringence domain. So, because of the very low entanglement density of PEEK, together with its high chain rigidity, uniaxial drawing above the glass transition temperature in the low-stress range can be compared with a flow process in which the orientational behaviour is predominant. At the onset of crystallization, which is certainly induced by the preferred orientation of the chain segments, the gradual build-up of a physically crosslinked network involves extension of the chains as the effect of the applied strain. Then, a second regime takes place at high strains, which is the deformation birefringence regime. The difference of strain birefringence already mentioned for PET and PMMA lies in the higher entanglement density and lower chain rigidity, which allow the stretching of the chains from the beginning of deformation. The result is that the stress-optical coefficient of PEEK to be used in the Kuhn and Grün model must be taken from the high-stress linear domain of *Figure 7*, not from the initial linear part as done in the case of PET.

The deformational stress-optical coefficient in the amorphous phase is then $[\Delta n_a/(1-X_c)]/\sigma = 4.4 \times 10^{-3}$ MPa^{-1} and, owing to knowledge of the optical anisotropy of the monomer unit calculated from the additive model of bond polarizabilities, $(\alpha_1-\alpha_2) = 1.175 \times 10^{-23}$ cm^{-3} where α_1 and α_2 are the polarizabilities of the monomer unit parallel and perpendicular to its molecular axis, respectively[41], one can estimate from equation (10) the number of monomer units per random link in PEEK, $N_0 \approx 1.2$. This result is perfectly consistent with the value of the shape factor of the rigid structural unit of the Brown–Windle model[42] that has been used in the second part of the work dealing with modelling the orientational behaviour[43]. Indeed, the curve-fitting procedure of the experimental data from both birefringence and shrinkage-stress measurements leads to the determination of a rigid structural unit, which is about three times as long as it is wide. This is roughly equivalent to a single PEEK monomer unit that is composed of three consecutive phenyl groups, the intercalated ether and ketone groups having only a minor contribution to the monomer length.

A comparison is worth making with the random link length, L, of various stiff-chain polymers such as poly(ethylene terephthalate) (PET), bisphenol A polycarbonate (PC) and poly(2,6-dimethyl-1,4-phenylene oxide) (PPO), which can be computed from the relation:

$$L = A^2 M_0/a_0 \qquad (11)$$

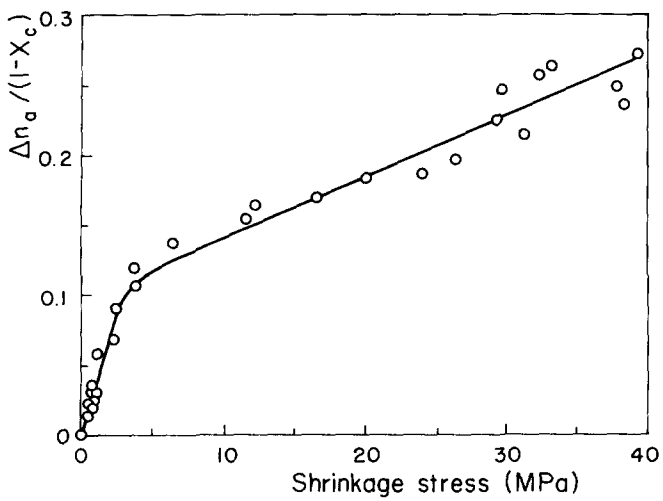

Figure 7 Amorphous birefringence contribution, $\Delta n_a/(1-X_c)$, *versus* shrinkage stress, σ, for the samples drawn from the amorphous state

Table 2 Molecular parameters for PET, PC and PPO as defined in equations (11) and (12)

	$A \times 10^4$ (nm $g^{-1/2}$ $mol^{1/2}$)	M_0 (g mol^{-1})	a_0[a] (nm)	L (nm)
PET	870±30	192	1.07	1.36
PC	900±30	254	1.04	1.98
PPO	840±10	120	0.48	1.76

[a] Assessed for the more stable conformation in the crystal: PET[45], PC[46] and PPO[47]

where M_0 is the molar weight of the monomer, a_0 is the length of the monomer unit projected on the local chain axis of the more stable conformation and A is a constant from the relation[44]:

$$(r_0^2)^{1/2} = AM^{1/2} \quad (12)$$

where $(r_0^2)^{1/2}$ is the root-mean-square end-to-end distance of the chains and M is the molar weight. *Table 2* gives the values of the various parameters of equation (11) for PET, PC and PPO, and the calculated values of the random link length, which compares very well with the value that can be estimated for PEEK, $L = 1.8$ nm, considering the extended monomer length $a_0 = 1.5$ nm[8,10]. It is to be noted that the slightly lower L value for PET is consistent with the lower chain rigidity mentioned previously.

Critical remark

The crosslinking effect of the crystallites originating from the strain-induced crystallization is the very phenomenon which allows use of the rubber network model to describe the orientational behaviour of PEEK because it prevents chain slippage. However, the accompanying filler effect of the crystallites is likely to perturb the rubber behaviour of the amorphous matrix of the composite material in comparison with a homogeneous rubbery material. The volume effect of the crystallites has been taken into consideration through the additivity law, as concerns the birefringence, and with the assumption of a uniform stress distribution, as concerns the shrinkage-stress behaviour. But the effect of the interparticle distance deserves some comments. Indeed, the amorphous matrix above T_g can only be considered as an ideal rubber network, from the standpoint of both birefringence and shrinkage stress, if the distance between the crosslinking particles is large compared with the length of the random link in order that the conformational and topological constraints imposed on the amorphous chains at their anchoring points on the crystallites quickly vanish and that little effect results on the overall behaviour of the amorphous matrix. In this connection, small-angle X-ray scattering measurements indicate that the average distance between the crystallites estimated from Bragg's law for the initially amorphous samples drawn at 160°C is about 13 nm, which is about one order of magnitude greater than the length of the random link. This vouches *a posteriori* for the rubber network model adopted in the present study.

CONCLUSION

The comparison of birefringence and infra-red dichroism data has led to the assessment of a value for the intrinsic birefringence of the amorphous phase, $\Delta n_a^\circ = 0.38$, significantly greater than that of the crystalline phase, as is generally the case for semicrystalline polymers. The strain-induced crystallization effect has been assigned to an orientational effect of the rigid structural units at low strains. The effectiveness of chain extension at the threshold of crystallization is due to the build-up of a physically crosslinked network as soon as a few crystals are capable of preventing chain slippage. The Gaussian statistical approach for the deformation of chain networks can be used to determine the molecular weight between entanglements from the elastic modulus at $\lambda \to 1$, and the length of the random link in the range $\lambda > 1.8$. The low average number of three entanglements per chain on average is perfectly consistent with the propensity of unravelling of the PEEK chains in the first stage of the deformation. The length of the random link of 1.8 nm is in very good agreement with the values that can be theoretically computed for several stiff-chain polymers closely related to PEEK from the standpoint of chemical structure.

REFERENCES

1 May, R. in 'Encyclopedia of Polymer Science and Engineering', Vol. 12 (Eds. H. M. Mark, N. M. Bikales, C. G. Overberger and G. Menges), Wiley, New York, 1988, pp. 313–320
2 Wilski, H., Pan, R., Cao, M.-Y. and Wunderlich, B. in 'Polymer Handbook', 3rd Edn. (Eds. J. Brandrup and E. H. Immergut), Wiley Interscience, New York, 1989, Ch. VII, pp. 371–407
3 Hoshino, S., Powers, J., Legrand, D. G., Kawai, H. and Stein, R. S. *J. Polym. Sci.* 1962, **58**, 185
4 Stein, R. S. in 'Newer Methods of Polymer Characterization' (Ed. B. Ke), Wiley Interscience, New York, 1964, Ch. 4
5 Wunderlich, B. 'Macromolecular Physics', Vol. 1, 'Crystal Structure, Morphology, Defects', Academic Press, New York, 1973, Ch. 4
6 Blundell, D. J. and Osborn, B. N. *Polymer* 1983, **24**, 953
7 Hay, J. N., Kemmish, D. J., Langford, I. I. and Rae, I. M. *Polym. Commun.* 1984, **25**, 175
8 Fratini, A. V., Cross, E. M., Whitaker, R. B. and Adams, W. W. *Polymer* 1986, **27**, 861
9 Wakelin, N. J. *J. Polym. Sci., Polym. Lett. Edn.* 1987, **25**, 25
10 Hay, J. N., Langford, I. I. and Loyd, J. R. *Polymer* 1989, **30**, 489
11 Séguéla, R. *Polymer* 1993, **34**, 1761
12 Samuels, R. J. 'Structured Polymer Properties', Wiley, New York, 1974, Ch. 2
13 Jasse, B. and Koenig, J. L. *J. Macromol. Sci., Rev. Macromol. Chem.* (C) 1979, **17**, 61
14 Ward, I. M. *Adv. Polym. Sci.* 1985, **66**, 81
15 Nguyen, H. X. and Ishida, H. *Polymer* 1986, **27**, 1400
16 Nguyen, H. X. and Ishida, H. *J. Polym. Sci., Polym. Phys. Edn.* 1986, **24**, 1079
17 Jonas, A., Legras, R. and Issi, J.-P. *Polymer* 1991, **32**, 3364
18 Varsanyi, G. 'Vibrational Spectra of Benzene Derivatives', Academic Press, New York, 1969
19 Chalmers, J. M., Gaskin, W. F. and Mackenzie, M. W. *Polym. Bull.* 1984, **11**, 433
20 Engelaere, J.-C., Cavrot, J.-P. and Rietsch, F. *Eur. Polym. J.* 1980, **16**, 721
21 Séguéla, R. and Rietsch, F. *Polym. Commun.* 1987, **28**, 256
22 Day, M., Deslandes, Y., Roovers, J. and Suprunchuk, T. *Polymer* 1991, **32**, 1258
23 Chien, M. C. and Weiss, R. A. *Polym. Eng. Sci.* 1988, **28**, 6
24 Mishra, A. K. and Schultz, J. M. *J. Appl. Polym. Sci.* 1989, **38**, 655
25 Lee, Y., Lefebvre, J.-M. and Porter, R. S. *J. Polym. Sci., Polym. Phys. Edn.* 1988, **26**, 795
26 Choy, C. L., Leung, W. P. and Nakafuku, C. *J. Polym. Sci., Polym. Phys. Edn.* 1990, **28**, 1965
27 Cakmak, M. *J. Polym. Sci., Polym. Lett. Edn.* 1989, **27**, 119
28 Rossignol, J.-M., Séguéla, R., Rietsch, F. and Dupuis-Lallemand, J. *J. Polym. Sci., Polym. Lett. Edn.* 1989, **27**, 527
29 Treloar, L. R. G. 'The Physics of Rubber Elasticity', 2nd Edn., Clarendon Press, Oxford, 1958

30 Prest, W. M. Jr and Porter, R. S. *J. Polym. Sci., Polym. Phys. Edn.* 1972, **10**, 1639
31 Donald, A. M. and Kramer, E. J. *J. Polym. Sci., Polym. Phys. Edn.* 1982, **20**, 899
32 Schmidt, L. R. *J. Appl. Polym. Sci.* 1979, **20**, 2463
33 Odajima, A. and Maeda, T. *J. Polym. Sci., Polym. Symp.* 1966, **15**, 54
34 Nakamae, K., Nishino, T. and Ohkubo, H. *J. Macromol. Sci., Phys. (B)* 1991, **30**, 1
35 Takayanagi, M., Imada, K. and Kajiyama, J. *J. Polym. Sci., Polym. Symp.* 1966, **15**, 263
36 Rietsch, F. *Eur. Polym. J.* 1985, **21**, 793
37 Kahar, N., Duckett, R. A. and Ward, I. M. *Polymer* 1978, **19**, 136
38 Kuhn, W. and Grün, F. *Kolloid Z.* 1942, **101**, 248
39 Cerf, R. *Fortschr. Hochpolym.-Forsch.* 1959, **1**, 382
40 Tsvetkov, V. N. in 'Newer Methods of Polymer Characterization' (Ed. B. Ke), Wiley Interscience, New York, 1964, Ch. 14
41 Kumar, S., Anderson, D. P. and Adams, W. W. *Polymer* 1986, **27**, 329
42 Brown, D. I. and Windle, A. H. *J. Mater. Sci.* 1984, **19**, 1997, 2013
43 Bassigny, V., Séguéla, R. and Rietsch, F. in preparation
44 Kurata, M. and Tsunashima, Y. in 'Polymer Handbook', 3rd Edn. (Eds. J. Brandrup and E. H. Immergut), Wiley Interscience, New York, 1989, Ch. VII, pp. 1–47
45 Daubeny, R. P. and Bunn, C. W. *Proc. R. Soc. Lond. (A)* 1954, **226**, 531
46 Bonart, R. *Makromol. Chem.* 1966, **92**, 149
47 Horokiri, S. *J. Polym. Sci., Polym. Phys. Edn.* 1972, **10**, 1172